

Probing the Evolution of IR Properties of $z \sim 6$ Quasars: *Spitzer* Observations

Linhua Jiang¹, Xiaohui Fan¹, Dean C. Hines², Yong Shi¹, Marianne Vestergaard¹, Frank Bertoldi³, W. N. Brandt⁴, Chris L. Carilli⁵, Pierre Cox⁶, Emeric Le Floch¹, Laura Pentericci⁷, Gordon T. Richards^{8,9}, George H. Rieke¹, Donald P. Schneider⁴, Michael A. Strauss⁸, Fabian Walter¹⁰, and J. Brinkmann¹¹

ABSTRACT

We present *Spitzer* observations of thirteen $z \sim 6$ quasars using the Infrared Array Camera (IRAC) and Multiband Imaging Photometer for *Spitzer* (MIPS). All the quasars except SDSS J000552.34–000655.8 (SDSS J0005–0006) were detected with high S/N in the four IRAC channels and the MIPS 24 μ m band, while SDSS J0005–0006 was marginally detected in the IRAC 8.0 μ m band, and not detected in the MIPS 24 μ m band. We find that most of these quasars have prominent emission from hot dust as evidenced by the observed 24 μ m fluxes. Their spectral energy distributions (SEDs) are similar to those of low-redshift quasars at rest-frame 0.15–3.5 μ m, suggesting that accretion disks and hot-dust structures for these sources already have reached maturity. However, SDSS J0005–0006 has an unusual SED that lies significantly below low-redshift SED templates at rest-frame 1 and 3.5 μ m, and thus shows a strong near-IR (NIR) deficit and no hot-dust emission. Type I quasars with extremely small NIR-to-optical flux ratios like SDSS J0005–0006 are not found in low-redshift quasar samples, indicating that SDSS J0005–0006 has different dust properties at high redshift. We combine the *Spitzer* observations with X-ray, UV/optical, mm/submm and radio observations to

¹Steward Observatory, University of Arizona, 933 North Cherry Avenue, Tucson, AZ 85721

²Space Science Institute, 4750 Walnut Street, Suite 205, Boulder, CO 80301

³Argelander Institute for Astronomy, University of Bonn, Auf dem Hügel 71, 53121 Bonn, Germany

⁴Department of Astronomy and Astrophysics, Pennsylvania State University, 525 Davey Laboratory, University Park, PA 16802

⁵National Radio Astronomy Observatory, P.O. Box 0, Socorro, NM 87801

⁶Institut de Radioastronomie Millimétrique, St. Martin d’Heres, F-38406, France

⁷Dipartimento di Fisica, Università degli Studi Roma 3, Via della Vasca Navale 84, Roma, Italy

⁸Department of Astrophysical Sciences, Peyton Hall, Princeton, NJ 08544

⁹Department of Physics and Astronomy, The Johns Hopkins University, 3400 North Charles Street, Baltimore, MD 21218

¹⁰Max-Planck-Institute for Astronomy, Königstuhl 17, D-69117 Heidelberg, Germany

¹¹Apache Point Observatory, P.O. Box 59, Sunspot, NM 88349

determine bolometric luminosities for all the quasars. We find that the four quasars with central black-hole mass measurements have Eddington ratios of order unity.

Subject headings: infrared: galaxies — galaxies: active — quasars: general — quasars: individual (SDSS J000552.34–000655.8)

1. INTRODUCTION

High-redshift quasars provide direct probes of the distant early universe where the first generation of galaxies and quasars formed. In the last few years, more than 20 luminous quasars at $z > 5.7$ have been discovered by the Sloan Digital Sky Survey (SDSS; York et al. 2000); the most distant one is at $z = 6.42$ (e.g. Fan et al. 2000, 2001, 2003, 2004, 2006). The discovery of these luminous objects at $z \sim 6$ reveals the existence of supermassive black holes (BHs) with masses higher than $10^9 M_\odot$ (e.g. Barth et al. 2003; Vestergaard 2004) in the first Gyr of cosmic history. These quasars provide a unique high-redshift sample to answer a series of challenging questions: How did the first billion-solar-mass BHs appear less than 1 Gyr after the Big Bang? How did they grow with time? Did the physical structure of quasars/AGNs evolve with time? Is the emission mechanism in quasars/AGNs the same at $z \sim 6$ as at $z \sim 0$? How were quasars and starburst activity related in the earliest galaxies? What is the role the quasar activity played in early galaxy evolution?

Understanding quasars requires observations from X-ray to radio wavelengths, each spectral region revealing different aspects of quasar emission and probing different regions of the active nuclei. One of the main results from the studies of $z \sim 6$ quasars is the apparent lack of strong evolution in their rest-frame UV/optical and X-ray properties. Their emission-line strengths and UV continuum shapes are very similar to those of low-redshift quasars (e.g. Barth et al. 2003; Pentericci et al. 2003; Fan et al. 2004), the emission line ratios indicate solar or supersolar metallicity in emission-line regions as found in low-redshift quasars (e.g. Hamann & Ferland 1999; Dietrich et al. 2003; Freudling et al. 2003; Maiolino et al. 2003), and the optical-to-X-ray flux ratios and X-ray continuum shapes show little evolution with redshift (e.g. Strateva et al. 2005; Vignali et al. 2005; Steffen et al. 2006; Shemmer et al. 2005, 2006). These measurements show that quasar accretion disks and emission-line regions are formed on very short time scales and their properties are not sensitive to the cosmic age.

However, it is not known whether this lack of evolution in high-energy spectral energy distributions (SEDs) at $z \sim 6$ extends to the rest-frame IR wavelength range. According to classical AGN unification models (Antonucci 1993), the accretion disk is surrounded by a dusty torus. Much of the emission from quasars/AGNs is re-processed by the dust and is re-emitted at IR wavelengths, where the quasar/AGN SEDs peak. The hottest dust lies within a few pc and produces near-IR (NIR) radiation, while warm and cool dust can extend to a few kpc and dominates the mid-IR (MIR) and far-IR (FIR) emission (e.g. Polletta et al. 2000; Nenkova et al. 2002; Siebenmorgen et

al. 2005). The individual contributions from AGN activity and star formation to the heating of warm/cool dust are poorly known (e.g. Wilkes 2001). On one hand, the shapes of the MIR-to-FIR SEDs indicate that AGN activity may dominate the heating of the warm/cool dust (e.g. Polletta et al. 2000; Haas et al. 2003). On the other hand, the radio-to-FIR correlation for star-forming galaxies (Condon 1992) still holds for most IR-luminous quasars out to the highest redshifts (e.g. Carilli et al. 2001, 2004), which suggests that the dust could be heated by starbursts in quasar host galaxies rather than quasar central engines. However, it is generally believed that emission from hot dust with temperature of $\sim 1000\text{K}$ is directly powered by central active nuclei (e.g. Rieke & Lebofsky 1981; Polletta et al. 2000; Haas et al. 2003), and thus is closely related to quasar activity.

The *Spitzer Space Telescope* (*Spitzer*; Werner et al. 2004) allows us, for the first time, to explore the rest-frame NIR range for high-redshift quasars and to constrain the evolution of hot dust in quasar environments. Hines et al. (2006) have observed thirteen $z > 4.5$ quasars using the Infrared Array Camera (IRAC; Fazio et al. 2004) and Multiband Imaging Photometer for *Spitzer* (MIPS; Rieke et al. 2004). They find that the SEDs of these high-redshift quasars at rest wavelength $0.6\text{--}4.3\ \mu\text{m}$ do not significantly differ from those of quasars with similar luminosity at low redshifts. In this paper, we report on *Spitzer* observations of thirteen $z \sim 6$ quasars discovered by the SDSS. All the quasars were observed with IRAC. Ten of them were also observed in the MIPS $24\mu\text{m}$ band, while the $24\mu\text{m}$ fluxes of the other three were taken from Hines et al. (2006).

In §2 of this paper, we present our high-redshift quasar sample and the *Spitzer* photometry of the thirteen quasars. In §3 we show their rest-frame NIR SEDs and study hot dust at $z \sim 6$. We calculate bolometric luminosities and accretion rates for these quasars in §4 and give the summary and discussion in §5. Throughout the paper we use λ_0 (ν_0) to denote rest-frame wavelength (frequency), and use a Λ -dominated flat cosmology with $H_0 = 70\ \text{km s}^{-1}\ \text{Mpc}^{-1}$, $\Omega_m = 0.3$ and $\Omega_\Lambda = 0.7$ (e.g. Spergel et al. 2003, 2006).

2. OBSERVATIONS

2.1. A fundamental sample of luminous $z \sim 6$ quasars from the Sloan Digital Sky Survey

The SDSS is the main source for high-redshift quasar discovery to date, and has discovered more than twenty luminous quasars at $z > 5.7$ from $\sim 8000\ \text{deg}^2$. Thirteen of them were observed using *Spitzer* and are included in this paper. Table 1 presents optical and NIR properties of the thirteen quasars. Redshifts, M_{1450} , m_{1450} , and the photometry in i , z , and J bands are mostly from the quasar discovery papers (Fan et al. 2000, 2001, 2003, 2004, 2006); K -band photometry of SDSS J1044–0125¹ is from Fan et al. (2000); H - and K' -band photometry of SDSS J1030+0524,

¹The naming convention for SDSS sources is SDSS JHHMMSS.SS±DDMMSS.S, and the positions are expressed in J2000.0 coordinates. We use SDSS JHHMM±DDMM for brevity.

J1048+4637, J1148+5251 and J1630+4012 are from Iwamuro et al. (2004); J -band photometry of SDSS J1044–0125 and H -band photometry of SDSS J0005–0006, J0836+0054, J0840+5624 and J1044–0125 were carried out in November 2005 using the 6.5m MMT with SWIRC, which is a J - and H -band camera operating at the f/5 cassegrain focus of the MMT. Note that the SDSS *ugriz* photometric system (Fukugita et al. 1996) is based on the AB magnitude scale of Oke & Gunn (1983), and that the photometry is reported on the asinh scale described in Lupton et al. (1999). The JHK measurements are Vega-based magnitudes.

These $z \sim 6$ quasars also have multiwavelength observations from radio (Petric et al. 2003; Carilli et al. 2004; Frey et al. 2005; Carilli et al. 2006), mm/submm (Petric et al. 2003; Priddey et al. 2003; Bertoldi et al. 2003a; Robson et al. 2004), to X-ray (Brandt et al. 2001, 2002; Bechtold et al. 2003; Farrah et al. 2004; Schwartz & Virani 2004; Shemmer et al. 2006). The *Spitzer* observations, combined with X-ray, optical, NIR, mm/submm and radio observations, provide a fundamental sample of quasar SEDs at $z \sim 6$.

2.2. *Spitzer* observations of thirteen $z \sim 6$ quasars

IRAC and MIPS $24\mu\text{m}$ photometry for the $z \sim 6$ quasars was obtained by our *Spitzer* GO-1 program (3198). IRAC observations were carried out in channels 1, 2, 3, and 4 (3.6, 4.5, 5.8 and $8.0\ \mu\text{m}$) with an exposure time of 1000 s in each channel. Images were processed by the IRAC Basic Calibrated Data (BCD) pipeline, and aperture photometry was performed using customized IDP3 (Schneider & Stobie 2002) IDL software. We used a 6 pixel ($7''.3$) target aperture radius and measured the background in an annulus from 8–13 pixels. The contaminant sources within the background area were masked by hand. Finally aperture corrections were derived from the *Spitzer* Tiny Tim simulations (Krist 2002). The pixel-to-pixel fluctuations in the background annuli were used to estimate the measurement uncertainties. In addition, there is an uncertainty of 3–5% in absolute calibration (Reach et al. 2005).

MIPS $24\mu\text{m}$ photometry for ten quasars was obtained in our *Spitzer* GO program, and the other three were observed in a MIPS GTO program (Hines et al. 2006). The integration time was 1400 s for quasars with high background, and 1260 s for others. The background is estimated using the *Spitzer* background estimator, and high background over the *Spitzer* $24\mu\text{m}$ passband is about 65.6 MJy/sr. Images were processed by the MIPS BCD pipeline and aperture photometry was performed in the same way as the procedure for IRAC. The target aperture radius was chosen to be 6 pixels ($15''.0$) and the background annulus from 8–13 pixels. The background fluctuations were also used to estimate the measurement uncertainties. The uncertainty in absolute calibration is about 10%.

Images at $70\ \mu\text{m}$ were obtained for four of the objects in the sample (2 from the GTO program and 2 from our GO program). These data were reduced with the MIPS Data Analysis Tool (Gordon et al. 2005). Photometry was performed using a $35''$ aperture with 39 – $65''$ background annulus.

None of the objects was detected at $70\ \mu\text{m}$. In order to increase the sensitivity of our measurements, we combined the observations into a median stacked image containing these four objects. While the measured noise decreased approximately by a factor of 2, no detection was achieved in the stacked image.

The observed fluxes and measurement uncertainties of the thirteen quasars are given in Table 2. The upper limits are constructed from the measured flux density in the target aperture plus two times the measurement uncertainty. All quasars except SDSS J0005–0006 were detected with high S/N in all IRAC bands and the MIPS $24\ \mu\text{m}$ band. SDSS J0005–0006 was marginally detected in the IRAC $8.0\ \mu\text{m}$ band, and not detected in the MIPS $24\ \mu\text{m}$ band. Because of its faintness, we use small apertures on this source (3 and 4 pixels respectively at 8.0 and $24\ \mu\text{m}$) to suppress noise; the measurements use appropriate aperture corrections. Figure 1 shows the IRAC and MIPS $24\ \mu\text{m}$ images for SDSS J0005–0006 (images in the second line) comparing with those of SDSS J0002+2550 (images in the first line), whose SED in the *Spitzer* bands is consistent with low-redshift SED templates (see §3 and Figure 2).

3. SPECTRAL ENERGY DISTRIBUTIONS AND HOT DUST AT HIGH REDSHIFT

3.1. Spectral Energy Distributions

Figure 2 shows the SEDs of the thirteen quasars from the *Spitzer* observations. Dotted lines are the average quasar SED from Elvis et al. (1994) and dashed lines are the SED template of luminous SDSS quasars from Richards et al. (2006). The SED templates have been normalized at rest-frame $1450\ \text{\AA}$. All these quasars have $[3.6]_{AB} - [4.5]_{AB} > -0.1$ ($[3.6]_{AB}$ and $[4.5]_{AB}$ are AB magnitudes at 3.6 and $4.5\ \mu\text{m}$, respectively), which is a MIR selection criterion for AGN used by Cool et al. (2006). The IRAC $4.5\ \mu\text{m}$ fluxes in some objects are significantly increased by strong $\text{H}\alpha$ emission lines. For most quasars, the continuum shapes at the wavelengths that the IRAC and MIPS $24\ \mu\text{m}$ bands cover ($0.5\ \mu\text{m} < \lambda_0 < 3.5\ \mu\text{m}$) are well predicted by the low-redshift SEDs. In a type I quasar, the radiation at $\lambda_0 < 1\ \mu\text{m}$ is from the accretion disk; at longer wavelengths of a few microns, emission from hot dust dominates over the disk emission. Figure 2 shows that even at $z \sim 6$, accretion disks and hot-dust structures for most quasars may already have reached maturity.

However, two quasars in this sample, SDSS J0005–0006 ($z = 5.85$) and SDSS J1411+1217 ($z = 5.93$), stand out as having unusual SEDs in this wavelength range: their fluxes at $24\ \mu\text{m}$ ($\lambda_0 \sim 3.5\ \mu\text{m}$) and/or $8\ \mu\text{m}$ ($\lambda_0 \sim 1\ \mu\text{m}$) significantly deviate from the low-redshift SEDs. For SDSS J1411+1217, the observed flux at $24\ \mu\text{m}$ is a factor of ~ 3 lower than that of the standard low-redshift templates. SDSS J0005–0006 is more extreme: it is marginally detected at $8\ \mu\text{m}$ and is completely undetected at $24\ \mu\text{m}$, at least an order of magnitude fainter than that predicted by the standard templates.

3.2. Hot dust in $z \sim 6$ quasars

We use a simple model to fit SEDs to our broad-band data at rest-frame $0.15\text{--}3.5\ \mu\text{m}$, consisting of a power-law disk component and a hot dust blackbody (Glikman et al. 2006). Glikman et al. (2006) find that a 1260K blackbody provides a good description of hot dust from their NIR quasar composite spectrum. Because only the $24\mu\text{m}$ fluxes are available to constrain hot dust for these $z \sim 6$ quasars, we fix the hot-dust temperature as 1260 K in our model fitting. Figure 3 shows the results of this fit. The dotted lines show the two components, and the dashed line is the sum of the two. The power-law slope α ($f_\nu \sim \nu^\alpha$) is also given in the figure. Most quasars have prominent hot-dust components seen as excess emission in the $24\mu\text{m}$ band, above the power-law disk components, while SDSS J0005–0006 and SDSS J1411+1217 do not show any hot-dust emission. The SED of SDSS J1411+1217 is consistent with a pure power-law over the full spectral range, and the fluxes of SDSS J0005–0006 at $\lambda_0 \sim 1$ and $3.5\ \mu\text{m}$ lie significantly below the power-law. At $z \sim 6$, quasar host galaxies are very young. It is possible that the properties of dust, including its temperature, composition and geometry, are different in such young objects from those at lower redshift (see §5 for a detailed discussion).

Radio and mm/submm (e.g. Bertoldi et al. 2003a; Priddey et al. 2003; Robson et al. 2004; Carilli et al. 2004) observations have revealed that these luminous $z \sim 6$ quasars have large amounts of warm/cool dust with masses higher than $10^8 M_\odot$. The warm/cool dust has temperatures from a few tens to a few hundred kelvins, while hot dust has temperatures of ~ 1000 K. In Figure 3 we fit the hot dust emission using a single-temperature blackbody, so we cannot calculate the hot-dust mass. However, we may estimate a lower limit to this mass by assuming that the hot dust radiates as a gray body. The dust mass M_d is determined by the following relation (Hughes et al. 1997),

$$M_d = \frac{F_1 D_L^2}{k_0 B(\nu_0, T_d)(1+z)}, \quad (1)$$

where F_1 is the observed flux density, D_L is the luminosity distance, k_0 is the rest-frame dust absorption coefficient, and $B(\nu_0, T_d)$ is the Planck function at rest frequency ν_0 and temperature T_d . We calculate the mass absorption coefficient k_0 according to Loeb & Haiman (1997) based on the extinction law of Mathis (1990). The lower limits of hot-dust masses are given in Figure 3.

In the analysis above we have neglected the contribution from the host galaxies of quasars. According to the correlation between central BH mass and host luminosity (Peng et al. 2006), the R -band luminosity is about $M_R = -24$ for a galaxy hosting a BH with a mass of a few $10^9 M_\odot$. Quasars with similarly massive BHs in our sample (see §4) are more luminous than $M_i = -27$. Using the elliptical galaxy template of Fioc & Rocca-Volmerange (1997), we find that the contribution from the host galaxies is expected to be less than 10% at rest-frame $1.6\ \mu\text{m}$, the peak of the template. We also use galaxy templates (Sbc, Scd, and Im) of Coleman et al. (1980), and find that the contribution from the host galaxies is less than 10% at rest-frame $5000\text{--}6000\text{\AA}$, the peak of the optical band in the templates.

Figure 4 shows the correlation between rest-frame 4400\AA luminosity and $3.5\mu\text{m}$ luminosity for

low- z type I quasars, compared with our measurements at high redshift (red points). We include PG quasars (green points; Schmidt & Green 1983) that were observed at $3.7\mu\text{m}$ (Neugebauer et al. 1987), $4.8\mu\text{m}$, $6.7\mu\text{m}$ or $7.3\mu\text{m}$ (Haas et al. 2000, 2003). We also include SDSS quasars (blue points) in the *Spitzer* Extragalactic First Look Survey and three *Spitzer* Wide-Area Infrared Extragalactic Survey areas (Richards et al. 2006). Cyan points present $z \sim 5$ quasars from Hines et al. (2006). Dashed lines show the best linear fit and its 3σ range. The correlation given in Figure 4 suggests that the dust emission at $3.5\mu\text{m}$ in quasars is heated directly by central engines (e.g. Rieke & Lebofsky 1981; Polletta et al. 2000; Haas et al. 2003). The NIR-to-optical flux ratios for most $z \sim 6$ quasars follow those at low redshift. However, SDSS J0005–0006 and SDSS J1411+1217 lie significantly below the linear fit. SDSS J1411+1217 is as IR-weak (IR-weak in this paper means small IR-to-optical ratios rather than weak absolute IR fluxes) as the most extreme examples at low redshift, while SDSS J0005–0006 is the most IR-weak object at any redshift in the figure. It is worth noting the quasars in Figure 4 are all typical type I quasars, and we do not consider other types of AGNs. For example, in Seyfert galaxies host galaxies may dominate the radiation at optical and IR wavelengths; while in blazars the optical emission could be boosted due to beaming effects, resulting in small IR-to-optical ratios.

3.3. Notes on individual objects

SDSS J000552.34–000655.8 ($z = 5.85$). SDSS J0005–0006 is selected from the SDSS Southern Survey, a deep survey repeatedly imaging the Fall Celestial Equatorial Stripe in the Southern Galactic Cap. It is the faintest quasar ($z_{AB} = 20.54$) in our sample. It also has the narrowest Ly α emission line of $z \sim 6$ quasars (Fan et al. 2004). This object is marginally detected in the IRAC $8.0\mu\text{m}$ band and is not detected in the MIPS $24\mu\text{m}$ band. Due to large measurement uncertainties, its SED is poorly constrained at both wavelengths. Further deep *Spitzer* observations, such as the IRAC $8.0\mu\text{m}$, the Infrared Spectrograph (IRS) Peak-Up Imaging $16\mu\text{m}$ and the MIPS $24\mu\text{m}$ photometry, are needed to place a strong constraint on its IR SED.

SDSS J083643.85+005453.3 ($z = 5.82$). SDSS J0836+0054 is the only known quasar at $z > 5.7$ detected by the Faint Images of the Radio Sky at Twenty-cm (FIRST; Becker et al. 1995). Its radio flux is variable. The flux at 1.4 GHz changed from 1.11 ± 0.15 mJy as measured by FIRST to 1.75 ± 0.04 mJy of Petric et al. (2003), a change of a factor of $\sim 60\%$, and the flux at 5 GHz changed from 0.58 ± 0.06 mJy of Petric et al. (2003) to 0.34 ± 0.06 mJy of Frey et al. (2005) by a factor of $\sim 70\%$. SDSS J0836+0054 has a strong and broad Ly α emission line (Fan et al. 2001) and a relatively weak MIPS $24\mu\text{m}$ flux.

SDSS J104433.04–012502.2 ($z = 5.74$). SDSS J1044–0125 is the first quasar discovered at $z > 5.7$ (Fan et al. 2000). It has weak X-ray emission (Brandt et al. 2001) and was confirmed to be a broad absorption line (BAL) quasar (Goodrich et al. 2001; Djorgovski et al. 2001). Submm observations at $850\mu\text{m}$ reveal the existence of $\sim 4 \times 10^8 M_{\odot}$ of cool dust in this object (Priddey et al. 2003). It is also bright at $24\mu\text{m}$, and thus has a large amount of hot dust.

SDSS J104845.05+463718.3 ($z = 6.20$). SDSS J1048+4637 is the most distant known BAL quasar (Maiolino et al. 2004b). It has been marginally detected at 1.4 GHz (Carilli et al. 2004), and not detected at 450 and 850 μm (Robson et al. 2004). Bertoldi et al. (2003a) detected it at 250 GHz and estimated a cool dust mass of $\sim 4 \times 10^8 M_{\odot}$ in this object. It was observed with IRS Peak-Up Imaging at 16 μm (Charmandaris et al. 2004), and the updated 16 μm flux is 0.49 mJy.

SDSS J114816.64+525150.2 ($z = 6.42$). SDSS J1148+5251 is the most distant quasar known. It has strong MIPS 24 μm output, indicating the existence of prominent hot dust. It was also detected at 450 and 850 μm (Robson et al. 2004), 250 GHz (Bertoldi et al. 2003a) and 1.4 GHz (Carilli et al. 2004). These observations show that it has copious cool dust with a mass of $5 - 7 \times 10^8 M_{\odot}$. CO observations (Bertoldi et al. 2003b; Walter et al. 2003, 2004) reveal the presence of $\sim 2 \times 10^{10} M_{\odot}$ of molecular gas in this object. It was also observed with IRS Peak-Up Imaging at 16 μm (Charmandaris et al. 2004), and its updated 16 μm flux is 0.84 mJy. Mahabal et al. (2005) discovered a very faint quasar RD J114816.2+525339 with $z_{AB} = 23.0$ at $z = 5.7$ near SDSS J1148+5251. We detected this faint source with IRAC at 3.6 and 4.5 μm with flux densities of 0.013 ± 0.002 and 0.013 ± 0.003 mJy, respectively, which are consistent with standard low- z SED templates.

SDSS J141111.29+121737.4 ($z = 5.93$). SDSS J1411+1217 has a very weak MIPS 24 μm flux, and its SED at $1 \mu\text{m} < \lambda_0 < 3.5 \mu\text{m}$ can be fitted with a pure power-law. It also has a narrow Ly α emission line (Fan et al. 2004).

4. BOLOMETRIC LUMINOSITIES AND ACCRETION RATES

Figure 5 presents the SEDs (filled circles) of the thirteen $z \sim 6$ quasars from X-ray to radio. The data other than our *Spitzer* observations are taken from the literature mentioned in §2.1. Filled circles with downward arrows are 2σ upper limits. Dotted lines are the average quasar SED from Elvis et al. (1994) and dashed lines are the SED template of luminous SDSS quasars from Richards et al. (2006). The templates have been normalized at IRAC 3.6 μm . Due to the anticorrelation between X-ray emission and optical luminosity in AGNs (e.g. Strateva et al. 2005; Steffen et al. 2006), the SED template of Richards et al. (2006) at X-ray band is well below that of Elvis et al. (1994) and the X-ray fluxes of the most luminous $z \sim 6$ quasars are often smaller than the Richards et al. (2006) template. After correcting for this effect, the X-ray emission from these $z \sim 6$ quasars is consistent with the low- z SED templates (Shemmer et al. 2006). To calculate bolometric luminosities, we first determine the full SED for each quasar. The SED between any two adjacent data points is interpolated using the Richards et al. (2006) mean SED, and the SED beyond the leftmost or rightmost points is directly scaled to this point using the mean SED. Table 3 gives the bolometric luminosities as well as optical and IR luminosities. Column 5 is the bolometric correction from rest-frame B band for all the quasars. The mean correction and standard deviation are 9.1 ± 2.2 , consistent with 11.8 ± 4.3 from Elvis et al. (1994) and 10.4 ± 2.5 from Richards et al. (2006).

We estimate central BH masses for the quasars that have been spectroscopically observed at rest-frame UV/optical wavelength (e.g. Goodrich et al. 2001; Barth et al. 2003) using the BH mass scaling relations (McLure & Dunlop 2004; Vestergaard & Peterson 2006). The BH mass of SDSS J0836+0054 is taken from Pentericci et al. (2006, in prep.) based on the relation of McLure & Dunlop (2004). Iwamuro et al. (2004) measured the MgII emission lines for four of the quasars. Due to low S/N, their measured MgII width for SDSS J1148+5251 is lower than that determined by Barth et al. (2003) by a factor of ~ 2 , which results in a factor of 4 lower estimated BH mass. We thus did not use the measurements of Iwamuro et al. (2004). The derived BH masses and Eddington luminosity ratios are given in Table 3. These luminous $z \sim 6$ quasars have supermassive BHs with masses of a few $10^9 M_{\odot}$ and Eddington ratios of order unity, comparable to quasars with similar luminosities at lower redshift (e.g. McLure & Dunlop 2004; Vestergaard 2004; Kollmeier et al. 2006).

5. SUMMARY AND DISCUSSION

We have carried out IRAC and MIPS $24\mu\text{m}$ photometry for thirteen $z \sim 6$ quasars. All the quasars except SDSS J0005–0006 were detected with high S/N in the IRAC and MIPS $24\mu\text{m}$ bands, while SDSS J0005–0006 was marginally detected in the IRAC $8.0\mu\text{m}$ band, and not detected in the MIPS $24\mu\text{m}$ band. The sample of the quasars is used to study the properties of IR SEDs and hot dust in high-redshift quasars. We find that the SEDs of most quasars follow low-redshift SEDs at the probed wavelengths. However, two quasars, SDSS J0005–0006 and SDSS J1411+1217, have unusual SEDs that lie significantly below the prediction of low-redshift SED templates at $24\mu\text{m}$ and/or $8\mu\text{m}$, showing a strong IR deficit. A simple model shows that most of the quasars have substantial hot dust, while the two IR-weak quasars do not show any hot-dust emission. We combine the *Spitzer* observations with X-ray, UV/optical, mm/submm and radio observations to determine bolometric luminosities for the high-redshift quasars. We find that these quasars have Eddington ratios of order unity.

It has been revealed that $z \sim 6$ quasars show a lack of evolution in their rest-frame UV/optical and X-ray SEDs. Our *Spitzer* observations show that, for most $z \sim 6$ quasars, NIR-to-MIR SEDs also do not differ significantly from those at low redshift. This suggests that accretion disks, emission-line regions and dust structures in most high-redshift quasars have reached maturity very early on. However, we found two quasars with a strong IR deficit. As shown in Figure 4, NIR-weak Type I quasars like SDSS J1411+1217 are very rare; and Type I quasars with extremely weak NIR fluxes like SDSS J0005–0006 are not found in a large sample at low redshift, but exist in a small sample of thirteen quasars at $z \sim 6$, suggesting that some quasars at high redshift may have different dust properties.

In the local universe, most dust in the ISM is produced by low and intermediate-mass AGB stars, which develop 0.5–1 Gyr after the initial starburst. At $z \sim 6$, the age of the universe is less than 1 Gyr, so quasar host galaxies are very young, with their first star formation likely to have

occurred less than half a Gyr earlier. The two NIR-weak quasars SDSS J0005–0006 and SDSS 1411+1217 could be too young to have formed dust tori around them, or perhaps, dust properties in such young systems differ from those of lower-redshift quasars. Thus the unusual IR SEDs of the two quasars may be a reflection of different dust properties in very young host galaxies at high redshift. Maiolino et al. (2004a) found that the dust extinction curve in quasar SDSS J1048+4836 ($z = 6.20$) is different from that observed at $z < 4$ (which is SMC-like, Hopkins et al. (2004)), implying a grain size distribution more similar to that expected from dust produced by supernovae. While other dust production mechanisms (e.g. Elvis et al. 2002) are also possible, it is currently unknown what their emission spectra are. SDSS J0005–0006 is especially interesting. If it has no hot dust, the observed SED at $1 \mu\text{m} < \lambda_0 < 3.5 \mu\text{m}$ comes from the disk only. This provides a strict constraint on disk models.

Hot dust in SDSS J0005–0006 and SDSS J1411+1217 could also be hidden by dust tori. According to AGN unification models, the accretion disk is surrounded by a dust torus. The hottest dust, with temperature more than 1000K, lies within a few pc, while cool dust with temperature of a few tens of kelvins can extend to a few kpc. As the angle between the torus axis and the line of sight increases, more hot dust could be hidden by the cool dust torus. Thus the hot-dust radiation in the NIR would be suppressed, and the $\lambda_0 \sim 1\mu\text{m}$ dip could be shifted toward longer wavelengths (Haas et al. 2003). Intriguingly, the emission line widths in the two NIR-weak quasars are the narrowest in our sample of $z \sim 6$ quasars. This suggests that the weak NIR SEDs in two sources could be caused by an obscuration with hot dust hidden by cooler dust tori. On the other hand, both objects show normal UV continuum and UV-to-X-ray flux ratio, and are thus not type II obscured objects in the normal sense, but could be intermediate objects in which the hot dust contribution is somewhat reduced. Further deep *Spitzer* observations are needed to constrain the SED shapes at $1\mu\text{m} < \lambda_0 < 4\mu\text{m}$, and NIR spectra are also needed to detect possible narrow line components.

We acknowledge support from NSF grant AST-0307384, a Sloan Research Fellowship and a Packard Fellowship for Science and Engineering (L.J., X.F., M.V.). We acknowledge support from NASA LTSA grant NAG5-13035 (WNB and DPS). We thank the SWIRC instrument team and MMT staff for their expert help in preparing and carrying out the SWIRC observing run.

This work is based on observations made with the Spitzer Space Telescope, which is operated by the Jet Propulsion Laboratory, California Institute of Technology under a contract (3198) with NASA. Support for this work was provided by NASA through an award issued by JPL/Caltech.

Funding for the SDSS and SDSS-II has been provided by the Alfred P. Sloan Foundation, the Participating Institutions, the National Science Foundation, the U.S. Department of Energy, the National Aeronautics and Space Administration, the Japanese Monbukagakusho, the Max Planck Society, and the Higher Education Funding Council for England. The SDSS Web Site is <http://www.sdss.org/>. The SDSS is managed by the Astrophysical Research Consortium for the Participating Institutions. The Participating Institutions are the American Museum of Natural

History, Astrophysical Institute Potsdam, University of Basel, Cambridge University, Case Western Reserve University, University of Chicago, Drexel University, Fermilab, the Institute for Advanced Study, the Japan Participation Group, Johns Hopkins University, the Joint Institute for Nuclear Astrophysics, the Kavli Institute for Particle Astrophysics and Cosmology, the Korean Scientist Group, the Chinese Academy of Sciences (LAMOST), Los Alamos National Laboratory, the Max-Planck-Institute for Astronomy (MPIA), the Max-Planck-Institute for Astrophysics (MPA), New Mexico State University, Ohio State University, University of Pittsburgh, University of Portsmouth, Princeton University, the United States Naval Observatory, and the University of Washington.

REFERENCES

- Antonucci, R., et al. 1993, *ARA&A*, 31, 473
- Barth, A. J., Martini, P., Nelson, C. H., & Ho, L. C. 2003, *ApJ*, 594, L95
- Bechtold, J., et al. 2003, *ApJ*, 588, 119
- Becker, R. H., White, R. L., & Helfand, D. J. 1995, *ApJ*, 450, 559
- Bertoldi, F., et al. 2003, *A&A*, 406, L55
- Bertoldi, F., et al. 2003, *A&A*, 409, L47
- Brandt, W. N., et al. 2001, *AJ*, 121, 591
- Brandt, W. N., et al. 2002, *ApJ*, 569, L5
- Carilli, C. L., Bertoldi, F., Omont, A., Cox, P., McMahon, R. G., & Isaak, K. G. 2001, *AJ*, 122, 1679
- Carilli, C. L., et al. 2004, *AJ*, 128, 997
- Carilli, C. L., et al. 2006, in preparation
- Charmandaris, V., et al. 2004, *ApJS*, 154, 142
- Coleman, G. D., Wu, C.-C., & Weedman, D. W. 1980, *ApJS*, 43, 393
- Condon, J. J. 1992, *ARA&A*, 30, 575
- Cool, R., J., et al. 2006, *AJ*, in press (astro-ph/0605030)
- Dietrich, M., Hamann, F., Appenzeller, I., & Vestergaard, M. 2003, *ApJ*, 596, 817
- Djorgovski, S. G., Castro, S., Stern, D., & Mahabal, A. A. 2001, *ApJ*, 560, L5
- Elvis, M., et al. 1994, *ApJS*, 95, 1

- Elvis, M., Marengo, M., & Karovska, M. 2002, *ApJ*, 567, L107
- Fan, X., et al. 2000, *AJ*, 120, 1167
- Fan, X., et al. 2001, *AJ*, 122, 2833
- Fan, X., et al. 2003, *AJ*, 125, 1649
- Fan, X., et al. 2004, *AJ*, 128, 515
- Fan, X., et al. 2006, *AJ*, 131, 1203
- Farrah, D., Priddey, R., Wilman, R., Haehnelt, M., & McMahon, R. 2004, *ApJ*, 611, L13
- Fazio, G., et al. 2004, *ApJS*, 154, 10
- Fioc, M., & Rocca-Volmerange, B. 1997, *A&A*, 326, 950
- Freudling, W., Corbin, M. R., & Korista, K. T. 2003, *ApJ*, 587, L67
- Frey, S., Paragi, Z., Mosoni, L., Gurvits, L. I. 2005, *A&A*, 436, L13
- Fukugita, M., Ichikawa, T., Gunn, J. E., Doi, M., Shimasaku, K., & Schneider, D. P. 1996, *AJ*, 111,1748
- Glikman, E., Helfand, D. J., & White, R. L. 2006, *ApJ*, 640, 579
- Goodrich, R. W., et al. 2001, *ApJ*, 561, L23
- Gordon, K. D., et al. 2005, *PASP*, 117, 503
- Haas, M., et al. 2000, *A&A*, 354, 453
- Haas, M., et al. 2003, *A&A*, 402, 87
- Hamann, F., & Ferland, G. 1999, *ARA&A*, 37, 487
- Hines, D. C., Krause, O., Rieke, G. H., Fan, X., Blaylock, M., & Neugebauer, G. 2006, *ApJ*, 641, L85
- Hopkins, P. F., et al. 2004, *AJ*, 128, 1112
- Hughes, D. H., Dunlop, J. S., & Rawlings, S. 1997, *MNRAS*, 289, 766
- Iwamuro, F., Kimura, M., Eto, S., Maihara, T., Motohara, K., Yoshii, Y., & Doi, M. 2004, *ApJ*, 614, 69
- Kollmeier, J. A., et al. 2006, *ApJ*, in press (astro-ph/0508657)
- Krist, J. 2002, *Tiny Tim/SIRTF User's Guide* (Pasadena: SSC)

- Loeb, A., & Haiman, Z. 1997, *ApJ*, 490, 571
- Lupton, R. H., Gunn, J. E., & Szalay, A. S. 1999, *AJ*, 118, 1406
- Mahabal, A., Stern, d., Bogosavljević, M., Djorgovski, S. G., & Thompson, D. 2005, *ApJ*, 634, L9
- Maiolino, R., Juarez, Y., Mujica, R., Nagar, N. M., & Oliva, E. 2003, *ApJ*, 596, L155
- Maiolino, R., et al. 2004, *Nature*, 431, 533
- Maiolino, R., Oliva, E., Ghinassi, F. Pedani, M., Mannucci, F., Mujica, R., & Juarez, Y. 2004, *A&A*, 420, 889
- Mathis, J. S. 1990, *ARA&A*, 28, 37
- McLure, R. J., & Dunlop, J. S. 2004, *MNRAS*, 352, 1390
- Nenkova, M., Ivezić, Ž., & Elitzur, M. 2002, *ApJ*, 570, L9
- Neugebauer, G., Green, R. F., Matthews, K., Schmidt, M., Soifer, B. T., & Bennett, J. 1987, *ApJS*, 63, 615
- Oke, J. B., & Gunn, J. E. 1983, *ApJ*, 266, 713
- Peng, C. Y., et al. 2006, *ApJ*, in press (astro-ph/0603248)
- Pentericci, L., et al. 2003, *A&A*, 410, 75
- Petric, A. O., et al. 2003, *AJ*, 126, 15
- Polletta, M., Courvoisier, T. J. -L., Hooper, E. J., & Wilkes, B. J. 2000, *A&A*, 362, 75
- Priddey, R. S., Isaak, K. G., McMahon, R. G., Robson, E. I., & Pearson, C. P. 2003, *MNRAS*, 344, L74
- Reach, W. T., et al. 2005, *PASP*, 117, 978
- Richards, G. T., et al. 2006, *ApJS*, in press (astro-ph/0601558)
- Rieke, G. H., & Lebofsky, M. J. 1981, *ApJ*, 250, 87
- Rieke, G. H., et al. 2004, *ApJS*, 154, 25
- Robson, I., Priddey, R. S., Isaak, K. G., & McMahon, R. G. 2004, *MNRAS*, 351, L29
- Schneider, G., & Stobie, E. 2002, in *ASP Conf. Ser. 281, Astronomical Data Analysis Software and Systems XI*, ed. D. A. Bohlender, D. Durand, & T. H. Handley (San Francisco: ASP), 382
- Schmidt, M., & Green, R. F., et al. 1983, *ApJ*, 269, 352

- Schwartz, D. A., & Virani, S. N. 2004, *ApJ*, 615, L21
- Siebenmorgen, R., Haas, M., Krügel, E., & Schulz, B. 2005, *A&A*, 436, 5L
- Shemmer, O., Brandt, W. N., Vignali, C., Schneider, D. P., Fan, X., Richards, G. T., & Strauss, M. A. 2005, *ApJ*, 630, 729
- Shemmer, O., et al. 2006, *ApJ*, 644, 86
- Spergel, D. N., et al. 2003, *ApJS*, 148, 175
- Spergel, D. N., et al. 2006, submitted to *ApJ* (astro-ph/0603449)
- Steffen, A. T., et al. 2006, *AJ*, 131, 2826
- Strateva, I. V., Brandt, W. N., Schneider, D. P., Vanden Berk, D. G., & Vignali, C. 2005, *AJ*, 130, 387
- Vestergaard, M. 2004, *ApJ*, 601, 676
- Vestergaard, M., & Peterson, B. M. 2006, *ApJ*, 641, 689
- Vignali, C., Brandt, W. N., Schneider, D. P., & Kaspi, S. 2005, *AJ*, 129, 2519
- Walter, F., et al. 2003, *Nature*, 424, 406
- Walter, F., et al. 2004, *ApJ*, 615, L17
- Werner, M. W., et al. 2004, *ApJS*, 154, 1
- Wilkes, B. J. 2001, *New Astronomy Reviews*, 45, 641
- York, D. G., et al. 2000, *AJ*, 120, 1579

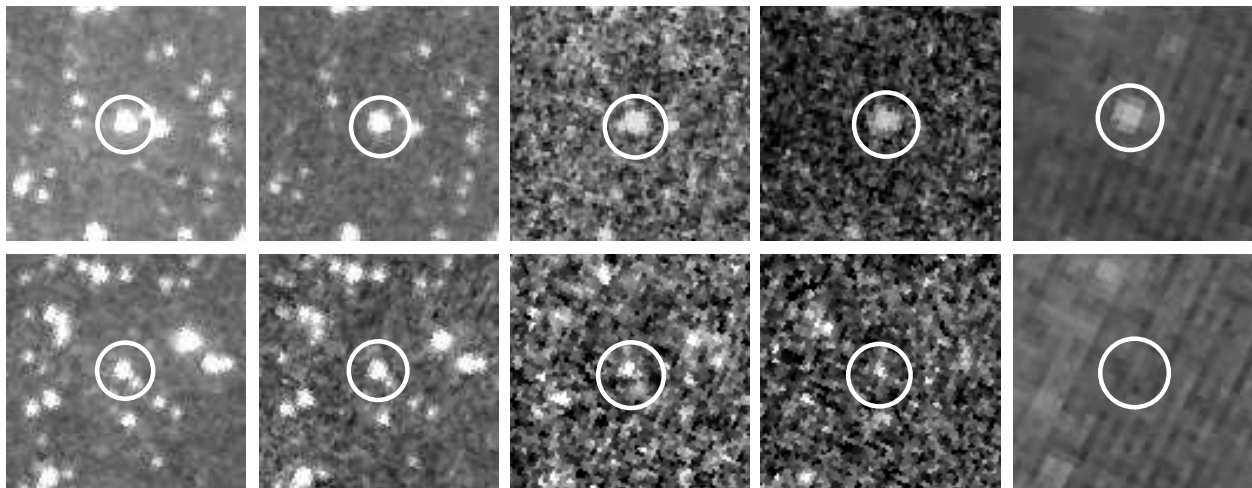


Fig. 1.— IRAC and MIPS $24\mu\text{m}$ images of SDSS J0005–0006 (images in the second line) compared with those of SDSS J0002+2550 (images in the first line), whose SED in the *Spitzer* bands is consistent with low-redshift SED templates (see §3 and Figure 2). The images from left to right correspond to IRAC channels 1, 2, 3 and 4, and the MIPS $24\mu\text{m}$ band. The size of the images is $1' \times 1'$. SDSS J0005–0006 was marginally detected in the IRAC $8.0\mu\text{m}$ band, and is not detected in the MIPS $24\mu\text{m}$ band.

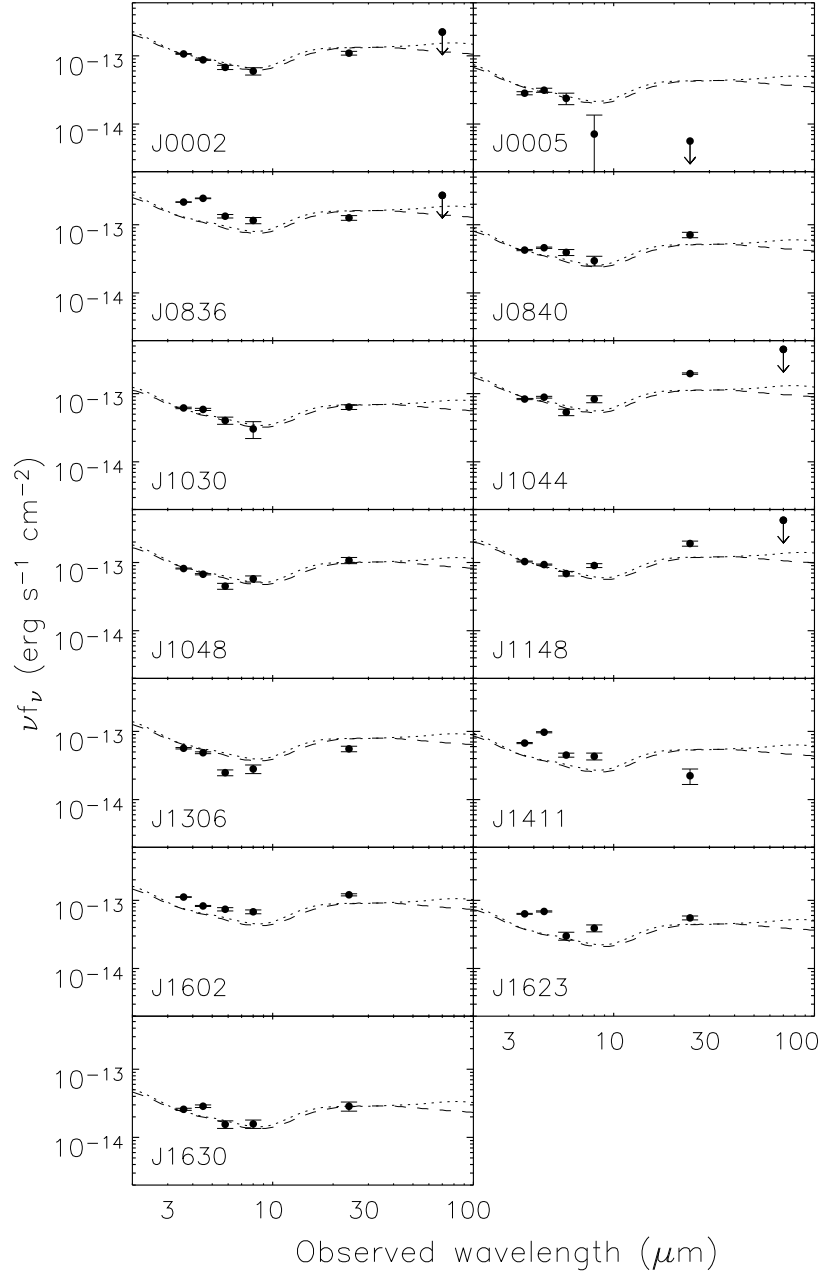


Fig. 2.— SEDs of the thirteen quasars from the *Spitzer* observations. The dotted and dashed lines are the average SEDs of type I low-redshift quasars from Elvis et al. (1994) and Richards et al. (2006), respectively, and have been normalized at rest-frame 1450 Å. Filled circles with downward arrows are 2σ upper limits. The measurement uncertainties are also given in the figure.

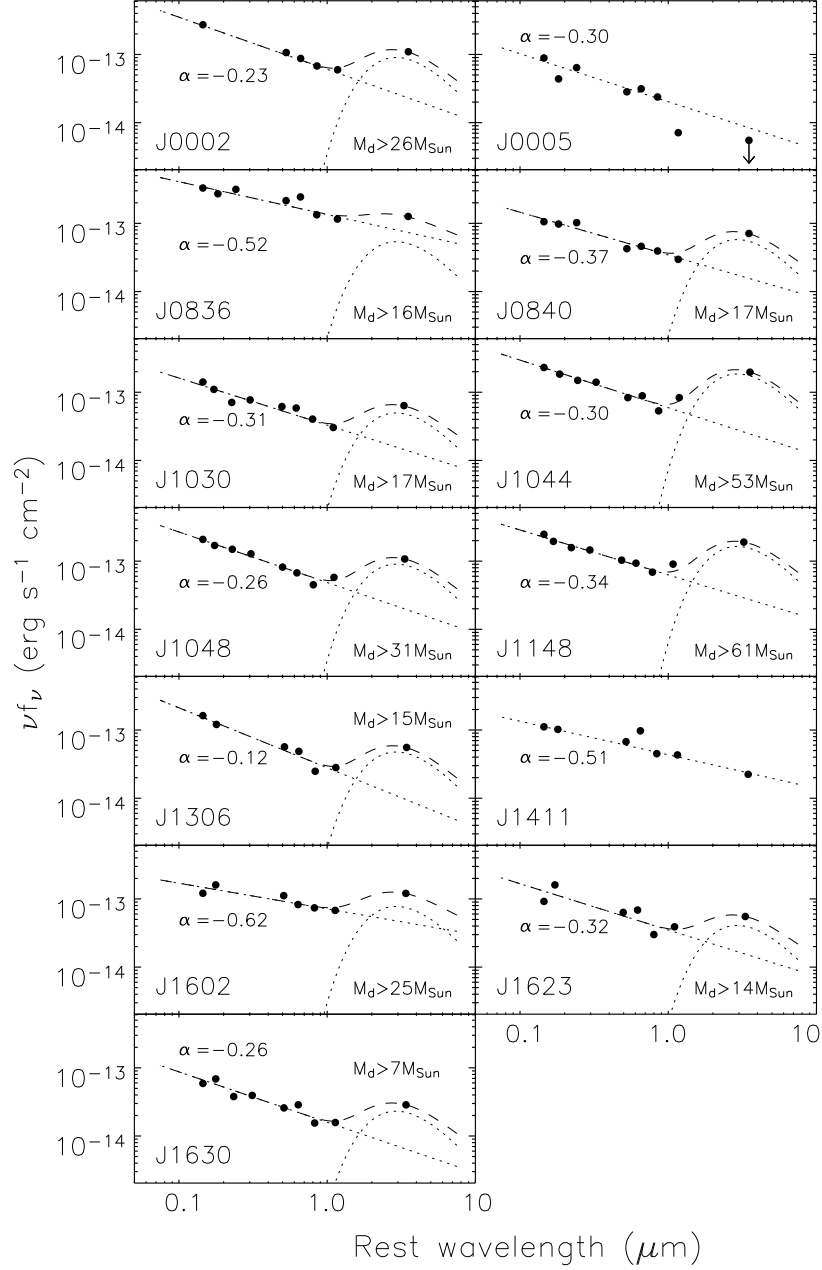


Fig. 3.— A simple model fitting to the high-redshift quasar SEDs at rest-frame 0.15 – 3.5 μm . The dotted lines in each panel show a power-law disk component and a blackbody component of hot dust, and the dashed line is the sum of the two. The power-law slope α and the lower limit of hot-dust mass M_d for each object are also given in the figure.

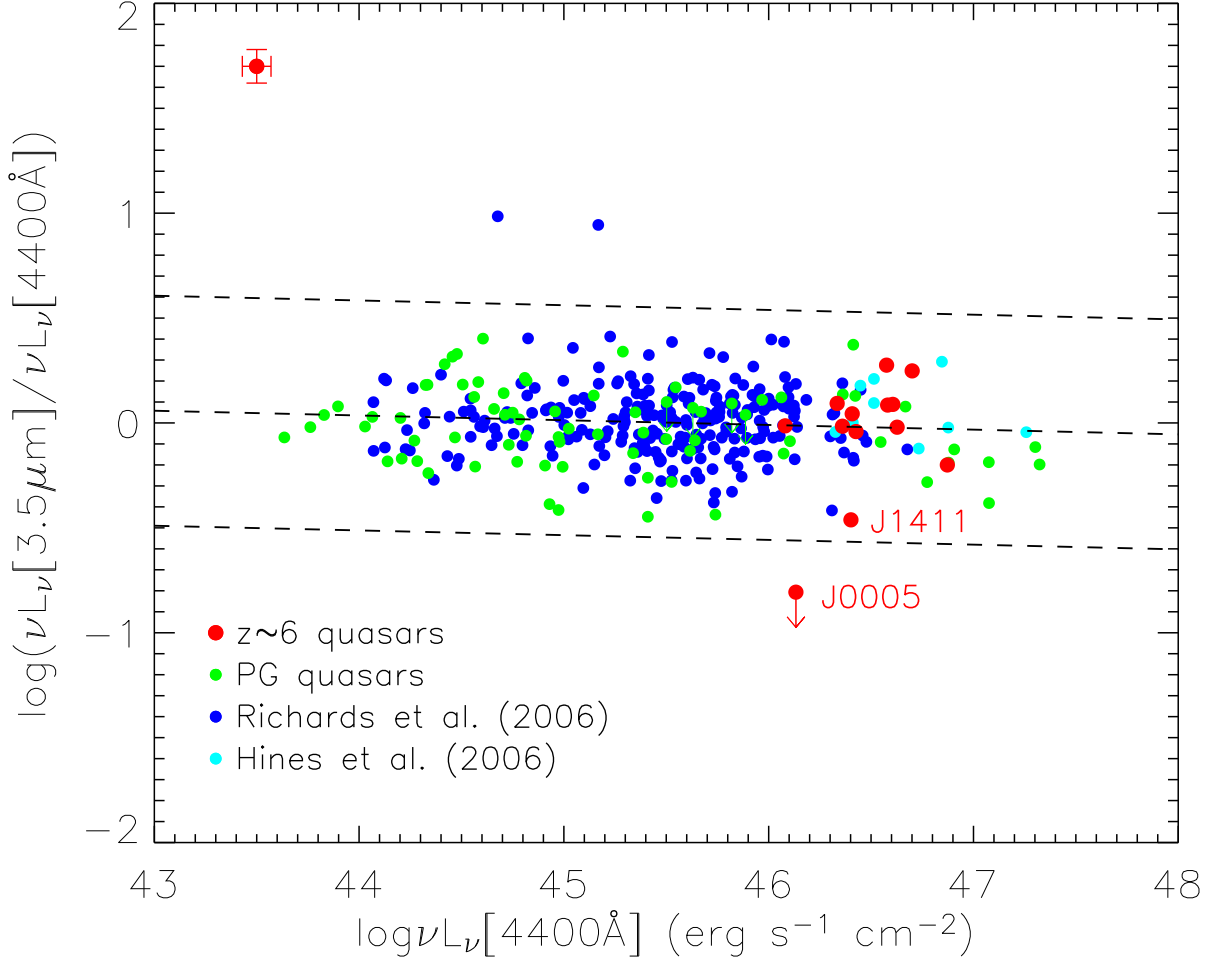


Fig. 4.— Correlation between rest-frame 4400\AA luminosity and $3.5\mu\text{m}$ luminosity for type I quasars. Red points are our $z \sim 6$ quasars. Green points are PG quasars (Schmidt & Green 1983) that were observed at $3.7\mu\text{m}$ (Neugebauer et al. 1987), $4.8\mu\text{m}$, $6.7\mu\text{m}$ or $7.3\mu\text{m}$ (Haas et al. 2000, 2003). Cyan points are $z \sim 5$ quasars from Hines et al. (2006). Filled circles with downward arrows are 2σ upper limits. Dashed lines show the best linear fit and its 3σ range. Typical errors for $z \sim 6$ quasars are given in the upper left corner. SDSS J1411+1217 is as IR-weak as the most extreme examples at low redshift, while SDSS J0005–0006 is the most IR-weak quasar at any redshift in the figure.

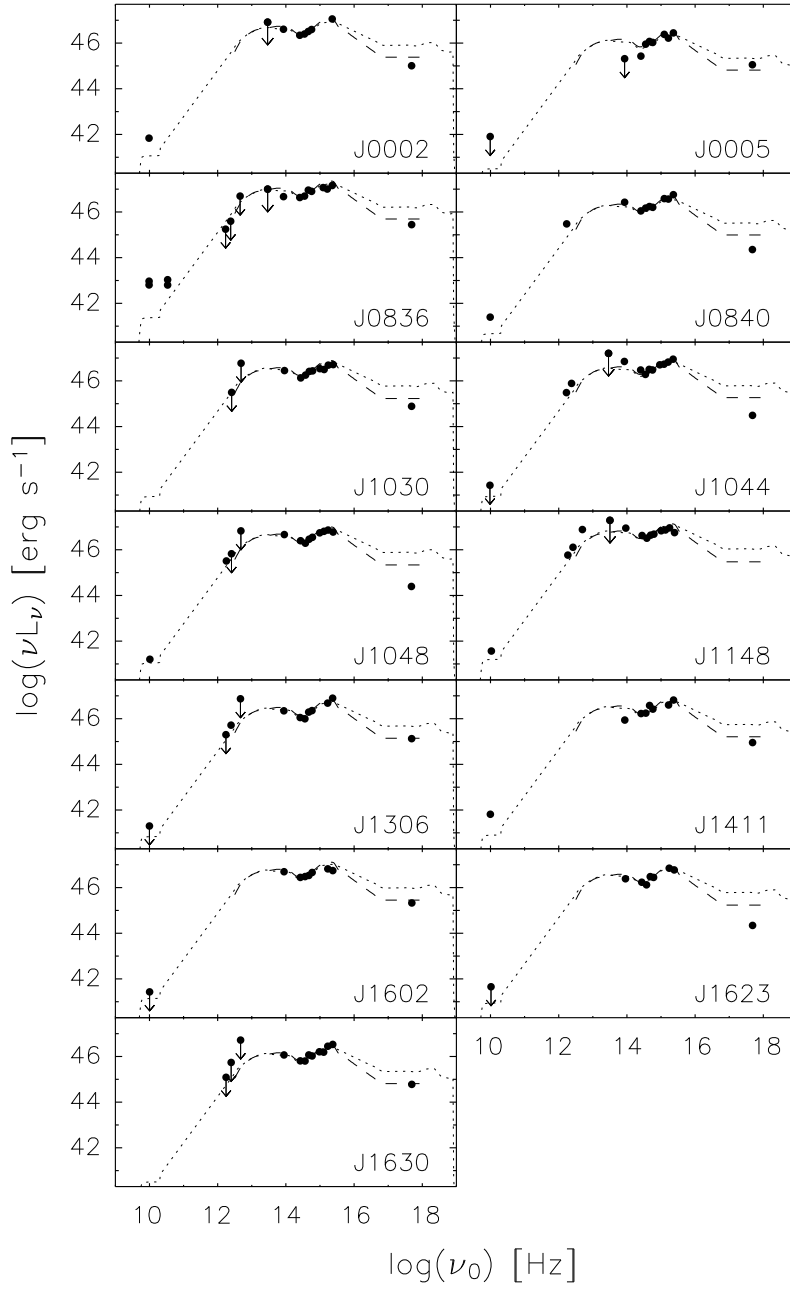


Fig. 5.— SEDs of the thirteen quasars from X-ray to radio. The data other than our *Spitzer* observations are taken from the literature mentioned in §2.1. Filled circles with downward arrows are 2σ upper limits. The dotted and dashed lines are the average SEDs of low-redshift quasars from Elvis et al. (1994) and Richards et al. (2006), respectively, and have been normalized at IRAC 3.6 μm ($\lambda_0 \sim 5000\text{\AA}$).

Table 1. Optical and NIR properties of the thirteen quasars

Quasar (SDSS)	redshift	M_{1450}	m_{1450}	i	z	J	H	K' (or K)	Ref.
J000239.39+255034.8	5.80	-27.7	19.02	21.47	18.99	4
J000552.34-000655.8	5.85	-26.2	20.23	23.40	20.54	19.87	18.68	...	4
J083643.85+005453.3	5.82	-27.9	18.81	21.04	18.74	17.89	16.95	...	2
J084035.09+562419.9	5.85	-26.9	20.04	22.43	19.76	19.00	18.17	...	5
J103027.10+052455.0	6.28	-27.2	19.66	23.23	20.05	18.87	18.57	17.67	2,6
J104433.04-012502.2	5.74	-27.5	19.21	21.81	19.23	18.31	17.76	17.02(K)	1
J104845.05+463718.3	6.20	-27.6	19.25	22.38	19.86	18.40	17.83	17.12	3,6
J114816.64+525150.2	6.42	-27.8	19.03	23.86	20.12	18.25	17.62	16.98	3,6
J130608.26+035626.3	5.99	-26.9	19.55	22.58	19.47	18.77	2
J141111.29+121737.4	5.93	-26.8	19.97	22.85	19.65	18.95	4
J160254.00+422825.0	6.07	-26.8	19.86	22.78	19.89	18.46	4
J162331.81+311200.5	6.22	-26.7	20.13	24.52	20.09	19.15	4
J163033.90+401209.6	6.05	-26.2	20.64	23.38	20.42	19.38	19.18	18.40	3,6

Note. — References (1) Fan et al. (2000); (2) Fan et al. (2001); (3) Fan et al. (2003); (4) Fan et al. (2004); (5) Fan et al. (2006); (6) Iwamuro et al. (2004). Redshifts, M_{1450} , m_{1450} , and the photometry in i , z , and J bands are mostly from the quasar discovery papers (Fan et al. 2000, 2001, 2003, 2004, 2006); K photometry of SDSS J1044-0125 is from Fan et al. (2000); H and K' photometry of SDSS J1030+0524, J1048+4637, J1148+5251 and J1630+4012 are from Iwamuro et al. (2004); J photometry of SDSS J1044-0125 and H photometry of SDSS J0005-0006, J0836+0054, J0840+5624 and J1044-0125 were carried out in November 2005 using the 6.5m MMT with SWIRC. The SDSS photometry of i and z is on the AB system; J , H , K and K' are on a Vega-based system.

Table 2. *Spitzer* photometry of the thirteen quasars

Quasar (SDSS)	3.6 μm (mJy)	4.5 μm (mJy)	5.8 μm (mJy)	8.0 μm (mJy)	24 μm (mJy)	70 μm (mJy) ^a
J0002+2550	0.128 \pm 0.002	0.131 \pm 0.002	0.131 \pm 0.009	0.159 \pm 0.019	0.876 \pm 0.055	5.21
J0005–0006	0.034 \pm 0.002	0.047 \pm 0.003	0.046 \pm 0.009	0.019 \pm 0.017 ^b	0.004 \pm 0.022 ^b	...
J0836+0054	0.258 \pm 0.003	0.366 \pm 0.004	0.258 \pm 0.015	0.308 \pm 0.032	1.010 \pm 0.080 ^c	6.29
J0840+5624	0.051 \pm 0.001	0.069 \pm 0.002	0.076 \pm 0.008	0.079 \pm 0.013	0.568 \pm 0.051	...
J1030+0524	0.074 \pm 0.002	0.088 \pm 0.003	0.078 \pm 0.009	0.081 \pm 0.023	0.509 \pm 0.041	...
J1044–0125	0.100 \pm 0.002	0.133 \pm 0.004	0.103 \pm 0.011	0.222 \pm 0.026	1.575 \pm 0.038	10.4
J1048+4637	0.098 \pm 0.002	0.101 \pm 0.002	0.087 \pm 0.009	0.154 \pm 0.016	0.860 \pm 0.090 ^c	...
J1148+5251	0.124 \pm 0.002	0.140 \pm 0.003	0.133 \pm 0.010	0.241 \pm 0.016	1.520 \pm 0.130 ^c	9.73
J1306+0356	0.068 \pm 0.002	0.073 \pm 0.002	0.048 \pm 0.005	0.075 \pm 0.011	0.444 \pm 0.041	...
J1411+1217	0.081 \pm 0.002	0.146 \pm 0.003	0.087 \pm 0.006	0.115 \pm 0.013	0.179 \pm 0.046	...
J1602+4228	0.134 \pm 0.001	0.124 \pm 0.002	0.143 \pm 0.008	0.181 \pm 0.012	0.964 \pm 0.034	...
J1623+3112	0.076 \pm 0.001	0.103 \pm 0.002	0.058 \pm 0.008	0.104 \pm 0.012	0.442 \pm 0.029	...
J1630+4012	0.031 \pm 0.001	0.043 \pm 0.002	0.030 \pm 0.004	0.042 \pm 0.006	0.229 \pm 0.035	...

Note. — Errors given in this table are measurement uncertainties only. The absolute calibration uncertainty for IRAC is 3–5%, and for MIPS is about 10%.

^a2 σ upper limits.

^bUsing smaller apertures than others for photometry; see §2.2.

^cFrom Hines et al. (2006).

Table 3: Optical, IR and bolometric luminosities for the thirteen quasars

Quasar (SDSS)	L_{Bol}^a	L_{Opt}^b	L_{IR}^c	$L_{Bol}/\nu L_\nu(4400\text{\AA})$	$M_{BH}(10^9 M_\odot)$	L_{Bol}/L_{Edd}
J0002+2550	47.57	47.19	47.18	8.5
J0005–0006	46.94	46.67	45.96	6.0
J0836+0054	47.72	47.36	47.28	7.0	6.8	0.54
J0840+5624	47.34	46.81	47.11	9.9
J1030+0524	47.37	46.91	47.04	8.7
J1044–0125	47.63	47.06	47.43	11.3	6.4	0.53
J1048+4637	47.55	47.08	47.29	9.1
J1148+5251	47.85	47.19	47.68	14.3	5.6	1.01
J1306+0356	47.40	46.94	47.04	10.3
J1411+1217	47.20	46.91	46.61	6.3
J1602+4228	47.59	47.13	47.27	9.6
J1623+3112	47.33	46.98	46.97	7.6	3.4	0.50
J1630+4012	47.06	46.57	46.75	9.8

^aBolometric luminosity (3cm to 10keV) in log(ergs/s).

^bOptical luminosity (0.1 μ m to 1.0 μ m) in log(ergs/s).

^cIR luminosity (1.0 μ m to 100.0 μ m) in log(ergs/s).